Available online at www.sciencedirect.com
SCIENCE DIRECT
Journal of Colloid and Interface Science 283 (2005) 380–384
JOURNAL OF Colloid and Interface Science
www.elsevier.com/locate/jcis

Preparation of ZnO colloids by aggregation of the nanocrystal subunits

L. Dong [a], Y.C. Liu [b,*], Y.H. Tong [b], Z.Y. Xiao [a], J.Y. Zhang [a], Y.M. Lu [a], D.Z. Shen [a], X.W. Fan [a]

[a] *Key Laboratory of Excited State Processes, Chinese Academy of Sciences, Changchun Institute of Optics, Fine Mechanics and Physics, No. 16 Eastern South-Lake Road, Changchun 130033, People's Republic of China*

[b] *Center for Advanced Optoelectronic Functional Material Research, Northeast Normal University, Changchun 130024, People's Republic of China*

Received 22 October 2003; accepted 13 September 2004

Abstract

Colloidal ZnO particles with narrow size distribution were prepared via a sol–gel process by base-catalyzed hydrolysis of zinc acetate. The morphology of ordered arrays of the particles was recorded by SEM. SEM also reveals that these uniform particles were composed of tiny ZnO subunits (singlets) sized of several nanometers. The size of the singlets, which is confirmed by X-ray diffraction and UV–vis absorption spectra, increases as the aging time is prolonged. The size-selective formation of colloids by aggregation of nanosized subunits is proposed to consist of two-stage growth by nucleation of nanosized crystalline primary particles and their subsequent aggregation into polycrystalline secondary colloids. The aggregates are all spherical because the internal rearrangement processes are fast enough. The ZnO colloids, i.e., the aggregates, tend to self-assemble into well-ordered hexagonal close-packed structures. Room-temperature photoluminescence was characterized for green and aged ZnO.

Keywords: Sol–gel processing; Colloidal ZnO particles; X-ray diffraction; UV–vis absorption spectrum; Scanning electron microscopy; Photoluminescence; Self-assembly

1. Introduction

In the past 10 years, research on quantum-sized semiconductor particles has increased enormously due to their exciting novel optical and electrical properties [1]. ZnO, a wide-band-gap semiconductor with a large exciton binding energy of 60 meV at room temperature, is rationally expected to be a promising candidate for room-temperature UV lasers or other interesting phenomena involving excited states. ZnO nanocrystals are an exceptionally important material for the envisaged applications in many technologies, such as solar energy conversion [2,3] and optoelectronic devices [4].

In addition to conventional physical methods, there have been several reports of solution-phase synthesis of ZnO colloids at low temperature, mainly based on the alcoholic hydrolysis of zinc precursors [5–7], hydrothermal methods [8], and electrochemical routes [9]. Among these techniques, the sol–gel route is very attractive because it is relatively easy to perform and allows us to tailor the morphology of particles by relative rate of hydrolysis and condensation reactions [10]. The method proposed by Spanhel and Anderson [5], hydrolysis of $Zn_4O(CH_3COO)_6$ precursors [11] formed in the first steps, is commonly used to synthesize ZnO nanocrystals. However, it was outlined that the nanoparticles obtained by this sol–gel route are not pure ZnO nanocrystals and that the presence of hydroxylated surfaces, with adsorbed water and organic molecules, can significantly affect material properties. Since the surface-related defects are both radiative and nonradiative decay channels to compete with the ZnO band-edge UV emission [12], the surface-bound molecules can influence emission properties of the ZnO particles [13].

Much research has been focused on the preparation and the properties of ZnO nanocrystals; however, little of it dealt with the aggregates of these nanosubunits, though the pioneering study of the growth of uniform inorganic particles

* Corresponding author. Fax: +86-431-4627031.
E-mail address: ycliu@nenu.edu.cn (Y.C. Liu).

0021-9797/$ – see front matter © 2004 Published by Elsevier Inc.
doi:10.1016/j.jcis.2004.09.044

by aggregation of small primary particles was published 35 years ago [14]. The driving force of the aggregation of small particles is believed to be correlated with the particle-size dependence of the interparticle potential [10,15]. Jezequel et al. reported a method for produce monodisperse ZnO spheres of various sizes [16]; however, this method resulted in polydisperse powders, according to Chang and co-workers [17]. Chang and co-workers developed this method to prepare monodisperse ZnO colloidal spheres for photonic crystals over a size range of ∼100–600 nm via a seeding process [17]. However, this method is not applicable for production of monodispersed ZnO spheres of sizes less than 100 nm.

In this work, we describe a simple method for producing ZnO colloidal spheres with narrow size distribution around 60 nm. These ZnO colloids proved to consist of nanosized ZnO subunits, which evolve with aging time. We also explore the luminescent properties of a powder specimen of the ZnO colloids.

2. Materials and methods

2.1. Reagents

All employed chemicals, if not mentioned exceptionally, were used as received without further purification. Zinc acetate dihydrate and all the solvents were purchased from Beijing Chemicals Co. Ltd. Lithium hydroxide monohydrate was purchased from Fluka. Ethanol was dehydrated by Lund and Bjezzum's method, utilizing the reactions with magnesium ethoxide [18].

2.2. Preparation and characterization

The ethanolic dispersions of ZnO nanoparticles were prepared following the same procedure developed by Spanhel and Anderson [5], except that some modifications were made, such as avoiding the supersonic stir and shift in growth temperature. For a typical preparation, 1.10 g $Zn(OAc)_2{\cdot}2H_2O$ was first dissolved in 50 ml absolute ethanol under vigorous stirring at 70 °C in a flask equipped with a condenser and a moisture trap and subsequently cooled to 50 °C. A stock solution of 0.29 g $LiOH{\cdot}H_2O$ in 50 ml absolute ethanol was then added to the $Zn(OAc)_2$ solution at 50 °C under constant stirring. Aliquots of solution were piped out by syringe at specific time during the growth process for further characterization. The solution remained clear until a slightly white precipitate occurred after about 60 min. Since hexane is commonly employed to precipitate CdSe, CdS, and ZnO nanocrystallites as an organic "nonsolvent" [6], hexane was adopted in our experiment to precipitate ZnO colloids. After the solution was rapidly cooled to 0 °C, hexane of three times the volume of the solution was added to precipitate the ZnO particles, followed by centrifugal separation at 10,000 rpm and washing with cold ethanol. When the reaction time is less than 10 min the solution remains clear after the addition of hexane. When it exceeds 20 min the addition of hexane induces a white cloudy solution. Powders for XRD and photoluminescent measurements were obtained by evaporating the remnant solvent from the precipitate. The precipitate was also redispersed in ethanol by ultrasonic stirring and then dipped onto the pretreated silicon wafer (n, 111) for SEM characterization. The treatment of the silicon wafer was performed according to a method published otherwise: the wafer was first cleaned in trichloroethane and then in a freshly prepared mixture of H_2SO_4 and H_2O_2 (30%) at a volume ratio of 4:1, followed by rinsing thoroughly with deionized water and drying at room temperature [19].

The absorption spectra of ZnO sol were obtained by a UV-360 recording spectrophotometer (Shimadzu). The size and morphology of ZnO samples were characterized by a field emission scanning electron microscope (Hitachi S4200) operating at 5 kV accelerating voltage. The crystalline structure of ZnO nanoparticles was characterized by X-ray diffraction using a rotating anode D/max-rA X-ray diffraction spectrometer (Rigaku) with Cu$K\alpha$ radiation at 1.54 Å. The room-temperature photoluminescent spectra were obtained on a Jobin Yvon UV-Labram Infinity spectrophotometer, excited by a continuous He–Cd laser at 325 nm with a power of 50 mW.

3. Results and discussions

Fig. 1 shows the absorbance spectra evolution for the synthesis of ZnO nanoparticles. All the spectra show well-defined exciton absorption peaks characteristic of ZnO, which have a significant blue-shift compared with that of the bulk ZnO, indicating that the average particle sizes are in the quantum size regime. The absorption onset red-shifts with aging time, indicating the growth (aging) of primary particles. The solution was transparent in the forepart of the growth time for about 60 min. Then the system changed into a blurred solution, and the absorption spectra exhibited significant background absorbance. The particle size can be determined from the absorption onset by the effective mass model [20]

$$E^* \cong E_g^{\text{bulk}} + \frac{\hbar^2\pi^2}{2er^2}\left(\frac{1}{m_e m_0} + \frac{1}{m_h m_0}\right), \tag{1}$$

where E^* is the band gap of the nanoparticle, E_g^{bulk} is the band gap of bulk material, r is the particle radius, m_e and m_h are the effective masses of the electrons and holes, respectively, and m_0 is the mass of a free electron. Although Eq. (1) is too simple for the ZnO system, it is widely used to survey particle size of ZnO in the quantum size regime ($\leqslant$7 nm), gaining results consistent with those from TEM and XRD [6]. Taking $m_e = 0.26$, $m_h = 0.59$, and $E_g^{\text{bulk}} = 3.2$ eV [21,22], the corresponding radius of zinc oxide nanoparticles with different aging times can be calculated, as shown in

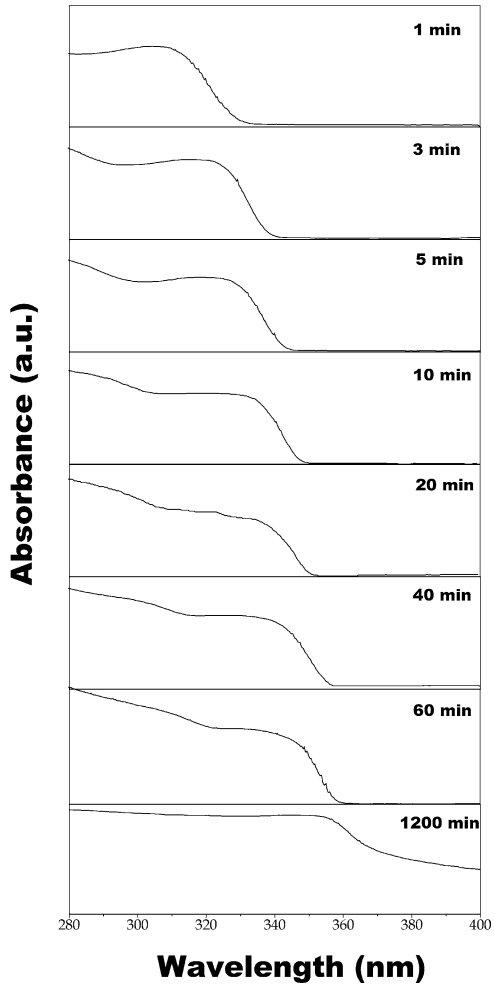

Fig. 1. UV–vis absorbance spectrum evolution with the aging time of zinc oxide nanoparticles.

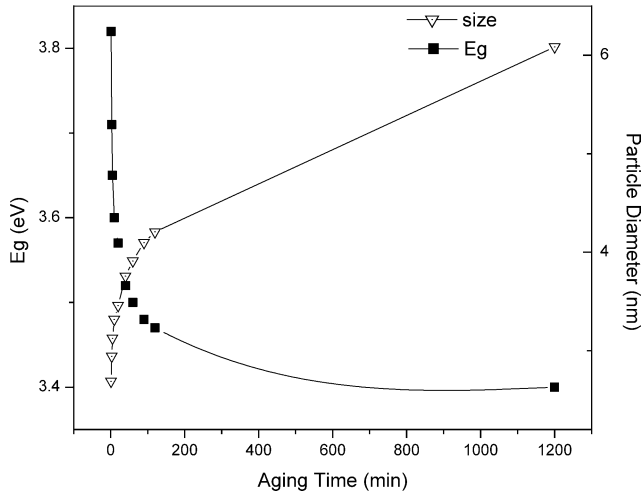

Fig. 2. Optical band gap evolution and the calculated particle diameter of the zinc oxide nanoparticles.

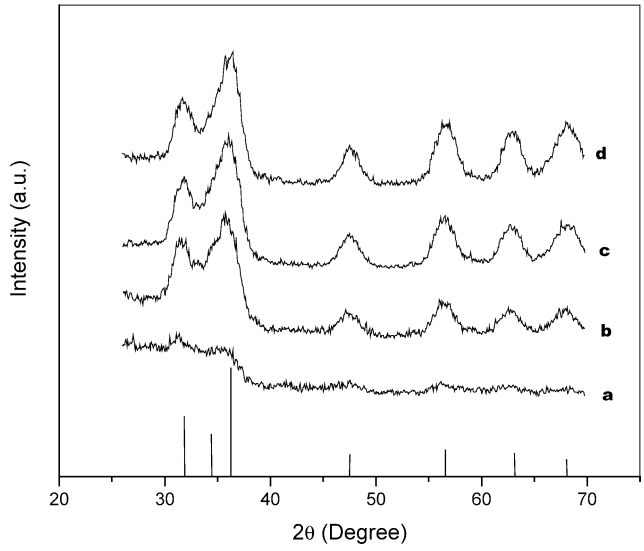

Fig. 3. Powder XRD patterns of the zinc oxide for (a) 40 min, (b) 60 min, (c) 120 min, and (d) 240 min.

Fig. 2. The results are relatively smaller than that estimated from XRD data by the Scherer formula. This divergence may be present for two reasons: one is that the centrifugal separations are more efficient for particles of larger sizes, resulting in larger sizes for powder specimens than for solution specimens; the other possibility may be the continuing growth process of the primary particles accelerated when the wet precipitates were desolvented because of the collapse of diffuse double layer. The latter factor may be dominant for the divergence in size because most of the primary particles have aggregated into spheres of narrow size distribution, sized at tens of nanometers, as confirmed from analysis of SEM. Therefore, primary particles of different sizes cannot be fractionally separated simply by centrifugal separation under our operation parameters.

Fig. 3 shows X-ray diffraction patterns of ZnO powder obtained at different growth times. By comparing the diffraction peak positions with those reported in the International Crystallographic data table, all the samples was assigned to be of a wurtzite structure with no preferential orientation. Fig. 3 shows an obvious decrease in full width at half maximum (FWHM) of the ZnO diffraction peaks with increased growth time, which correlates well with an increase in the average nanocrystal size. FWHM of the (110) diffraction peak are $1.875° \pm 0.038°$, $1.767° \pm 0.040°$, $1.685° \pm 0.054°$, and $1.354° \pm 0.171°$ for the samples taken at 40, 60, 120, and 240 min, respectively.

The morphology of ZnO particles is characterized by field emission microscopy, as shown in Fig. 4. Fig. 4A clearly reveals the presence of monomers and oligomers of ZnO singlets in the solution during the initial stages, having an approximate diameter of 3–4 nm, consistent with that estimated by optical absorption spectra. Therefore, the singlets are assumed to be each a nanocrystal that grows slightly during the aging process. The singlets also assembled into oligomeric aggregates.

Spheres formed by aggregation of these singlets are shown in Fig. 5 at two different magnifications of the same specimen shown in Fig. 4A. As shown in the inset of Fig. 5,

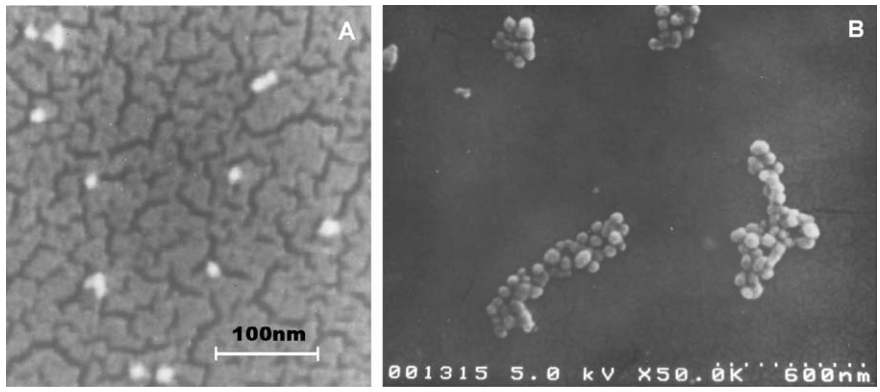

Fig. 4. SEM image of ZnO particles: (A) monomer and oligomer of ZnO singlets and (B) spheres after 40 min of aging.

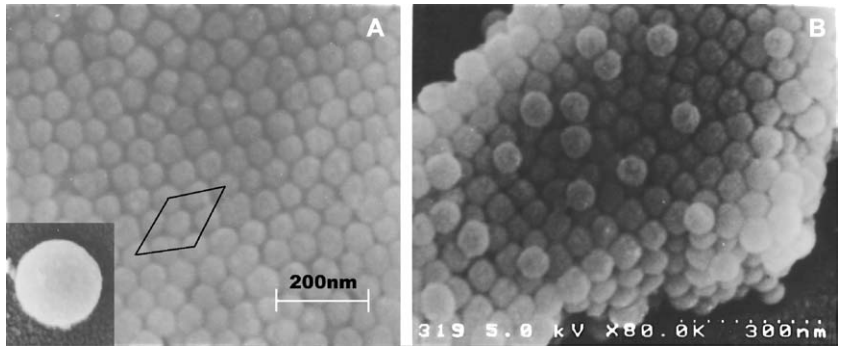

Fig. 5. Self-assembly of ZnO spheres on silicon, illustrating hexagonal packing: (A) the well-ordered facade and (B) the flank of a cluster of ZnO spheres.

the colloidal spheres, namely the secondary particles that have an average diameter of about 60 nm, are obviously constructed with the singlets shown in Fig. 4A. SEM observation of the aliquots before precipitation by hexane results in the same morphology, which indicates that the colloidal spheres had already formed before they were piped out. The ZnO spheres of narrow size distribution are inclined to assemble into ordered structures after the solution containing ZnO sols is dropped onto a silicon substrate, as shown in Figs. 5A and 5B. Fig. 5A shows the well-ordered facade of the close-packed aggregates. In Fig. 4B, the flank of the cluster of ZnO spheres reveals the three-dimensional structure of hexagonal lattice. Separated spheres are scarcely found with SEM observation and nearly all of the ZnO spheres ($\geqslant$99%) we observed are in multilayered form because of the surface tension of the solvent during evaporation.

The size-selective formation of colloids by aggregation of nanosized subunits has been investigated by Matijevic and co-workers [23,24], using either monodisperse spherical CdS or gold sols as the model system. The mechanism is proposed to consist of two-stage growth by nucleation of nanosized crystalline primary particles and their subsequent aggregation into polycrystalline secondary colloids. The aggregates are all spherical because the internal rearrangement processes are fast enough. Fig. 4B depicts the morphology of ZnO secondary colloids aged for 40 min. Ripening caused obvious fusion between the necks and the distortion of secondary particles from sphericity by dissolution and reprecipitation. The secondary colloids then have been irreversibly connected with each other in the reaction system and are not suitable for self-assembly any more.

The rate of ripening can be influenced by several factors, such as temperature, pH, and concentration, some of which may also affect the formation of the monodispersed colloids. Therefore, further research into the influence of these factors on the formation of monodisperse colloids is under progress.

Room-temperature photoluminescence of ZnO powder is given in Fig. 6. The ratio of UV emission intensity to green emission intensity increases with the increase of aging time. Since UV emission is assigned to recombination of bound excitons, while green emission is assigned to the recombination of electrons in singly occupied oxygen vacancies with photoexcited holes [11], the increase in the ratio of UV emission to visible emission indicates an improvement of the crystal quality of the nanoparticles; i.e., a decrease in the density of surface defects happens during the aging process via Ostwald ripening. There are obvious blue shifts in UV emission peak position compared with that estimated for the bulk ZnO as a result of the quantum-confined effect. The extent of this blue shift decreases as the size of the primary particles increases during the aging process.

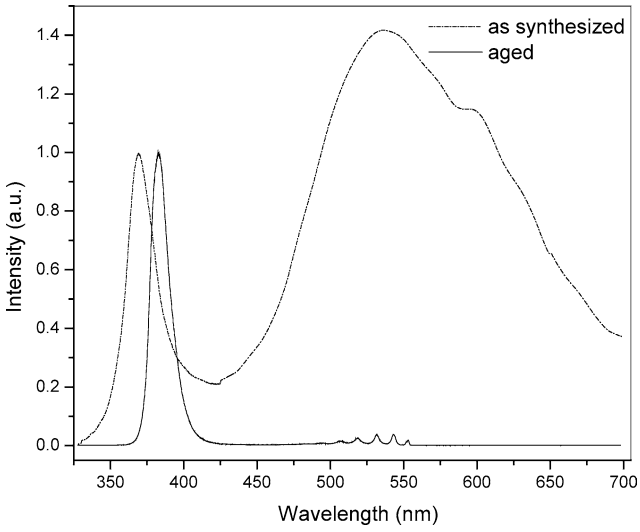

Fig. 6. Room-temperature photoluminescent spectra for ZnO as synthesized and aged for 40 min.

4. Conclusions

Colloidal ZnO spheres of narrow size distribution consisting of nanosized ZnO primary particles were synthesized by sol–gel methods. The size of the primary particles can be calculated from the optical band or from powder XRD pattern. The morphology and the narrow size distribution of the colloidal spheres can be maintained if the solution is stored at low temperature. These ZnO colloids arranged into a close-packed fcc periodic array. Room-temperature photoluminescence of ZnO powder show an increase in the ratio of UV emission intensity to green emission intensity with increased aging time, indicating an improvement of the crystal quality of the nanoparticles during the aging process. The extent of this blue shift decreases as the size of the primary particles increases during the aging process.

Acknowledgments

This work is supported by the Program of CAS Hundred Talents, the Innovation Project Item of Chinese Academy of Science, the National Natural Science Foundation of China (60176003, 60376009, and 60278031), and the National High Technique Program “863.”

References

[1] M.L. Cohen, Annu. Rev. Mater. Sci. 30 (2000) 1.
[2] H. Rensmo, K. Keis, H. Lindstrom, A. Solbrand, A. Hagfeldt, S.E. Lindquist, L.N. Wang, M. Muhammed, J. Phys. Chem. B 101 (1997) 2598.
[3] C. Bauer, G. Boschloo, E. Mukhtar, A. Hagfeldt, J. Phys. Chem. B 105 (2001) 5585.
[4] X.T. Zhang, Y.C. Liu, L.G. Zhang, J.Y. Zhang, Y.M. Lu, D.Z. Shen, W. Xu, G.Z. Zhong, X.W. Fan, X.G. Kong, J. Appl. Phys. 92 (2002) 3293.
[5] L. Spanhel, M.A. Anderson, J. Am. Chem. Soc. 113 (1991) 2826.
[6] E.A. Meulenkamp, J. Phys. Chem. B 102 (1998) 5566.
[7] E. Wong, J.E. Bonevich, P.C. Searson, J. Phys. Chem. B 102 (1998) 7770.
[8] J. Zhang, L. Sun, J. Yin, H. Su, C. Liao, C. Yan, Chem. Mater. 14 (2002) 4172.
[9] R.M. Nyffenegger, B. Craft, M. Shaaban, S. Gorer, G. Erley, R.M. Penner, Chem. Mater. 10 (1998) 1120.
[10] C.J. Brinker, G.W. Scherer, Sol–Gel Science: The Physics and Chemistry of Sol–Gel Processing, Academic Press, San Diego, 1990.
[11] M.S. Tokumoto, S.H. Plcinelli, C.V. Santilli, V. Briois, J. Phys. Chem. B 107 (2003) 568–574.
[12] A. Van Dijken, E.A. Meulenkamp, D. Vanmaekelbergh, A. Meijerink, J. Phys. Chem. B 104 (2000) 1715.
[13] S. Sakohara, M. Ishida, M.A. Anderson, J. Phys. Chem. B 102 (1998) 10,169.
[14] J.J. Petres, Gj. Dezelic, B. Tezak, Croat. Chem. Acta 41 (1969) 183–186.
[15] E. Matijevic, in: L.L. Hench, D.R. Ulrich (Eds.), Science of Ceramic Chemical Processing, Wiley, New York, 1986, pp. 463–481.
[16] D. Jezequel, J. Guenot, N. Jouini, F. Fievet, Mater. Sci. Forum 339 (1994) 152.
[17] E.W. Seelig, B. Tang, A. Yamilov, H. Cao, R.P.H. Chang, Mater. Chem. Phys. 80 (2003) 257.
[18] D.D. Perrin, W.L.F. Armarego, Purification of Laboratory Chemicals, fourth ed., Butterworth–Heinemann, Oxford, 1997, p. 209.
[19] C. Wang, Y. Zhang, L. Dong, L. Fu, Y. Bai, T. Li, J. Xu, Y. Wei, Chem. Mater. 12 (2000) 3662–3666.
[20] L.E. Brus, J. Chem. Phys. 79 (1983) 5566.
[21] L.I. Berger, Semiconductor Materials, CRC Press, Boca Raton, FL, 1997, p.184.
[22] S.M. Sze, Physics of Semiconductor Devices, Wiley, New York, 1981, p. 849.
[23] V. Privman, D.V. Goia, J. Park, E. Matijevic, J. Colloid Interface Sci. 213 (1999) 36.
[24] S. Libert, V. Gorshkov, V. Privman, D. Goia, E. Matijevic, Adv. Colloid Interface Sci. 100–102 (2003) 169.